Journal of Alloys and Compounds 501 (2010) 282–290

Contents lists available at ScienceDirect

Journal of Alloys and Compounds

journal homepage: www.elsevier.com/locate/jallcom

Experimental study and phase diagram calculation in Al–Zn–Mg–Si quaternary system

Qian Li[a,*], Yang-Zi Zhao[a], Qun Luo[a], Shuang-Lin Chen[a,b], Jie-Yu Zhang[a], Kuo-Chih Chou[a,c]

[a] Shanghai Key Laboratory of Modern Metallurgy & Materials Processing, Shanghai University, Shanghai 200072, China
[b] CompuTherm, LLC, Madison, WI 53719, USA
[c] Department of Physical Chemistry, University of Science and Technology Beijing, Beijing 100083, China

ARTICLE INFO

Article history:
Received 16 November 2009
Received in revised form 11 April 2010
Accepted 14 April 2010
Available online 22 April 2010

Keywords:
Coating materials
Phase diagrams
Computer simulations

ABSTRACT

The phase equilibrium of the Al–Zn–Mg–Si quaternary system containing (Al), (Si), $MgZn_2$ and Mg_2Si phases has been studied by means of scanning electron microscopy (SEM), electron dispersive spectrometry (EDS), X-ray diffraction (XRD) and differential scanning calorimeter (DSC) as well as calculation of phase diagram based on PANDAT software. Two three-phase fields and one four-phase field among the 15 wt% Al–Zn–Mg–6 wt% Si alloys in the concentration of Zn ranging from 57 wt% to 67 wt% have been confirmed at 573 K. The result showed non-existence of quaternary compound in this region. Based on the experimental results, the appropriate thermodynamic description of Mg–Si system was chosen. The ternary interactions in the liquid phase of Al–Mg–Si and Mg–Zn–Si systems have been assessed and the calculated ternary phase diagrams agreed well with the experimental data. Combining with the related ternary systems, the thermodynamic description of the Al–Zn–Mg–Si system was presented, and the good agreement between the calculated results and the experimental results was obtained.

1. Introduction

Steel is one of the major materials used in many areas. As one of the main methods to protect steel products from oxidation and corrosion, the hot-dip coating of aluminum–zinc based alloys has been used widely. During the past decade, the use of metallic coated steels in automotive, construction and appliance applications has increased at a greater rate than the overall growth in the steel industry. Microalloying elements in aluminum–zinc based alloys alter properties by changing the morphology, chemistry, structure, spatial distribution and size of precipitates. It was found that Mg, Si and RE (rare-earth) as alloying elements can significantly improve characteristics of the Al–Zn based alloy, such as AZ alloy [1–3] and alloy coating [2,4]. The solid solution phases (Al) and (Si) and the intermetallics Mg_2Si and $MgZn_2$ are able to improve the wear resistance of Al–Zn based alloy and the corrosion resistance of the hot-dip Al–Zn alloy coating. In the work of Tanaka et al. [5], Mg and Si in the outer adhered layer and Si in the inner alloy layer make the Zn–6Al–0.5Mg–0.1Si (in weight pct) coating more anti-corrosive. Morimoto et al. [6] found that the increase of Al, Mg contents in coating and the addition of Si improved corrosion resistance of the coating in salt spray tests. It is well known that for successful development of new materials and improvement of existing Al–Zn based alloys, the knowledge of phase diagrams and thermodynamic data is fundamental. Phase equilibria of the Al–Zn–Mg–Si quaternary system provide crucial information in development and design of AZ alloys. Some experimental work of the Al–Zn–Mg–Si system is available in literature. Yuan et al. [7] reported that the grain sizes of Sb or Ca modified Al–Zn–Mg–Si alloys were much finer than that of base alloy, and thought that no ternary compound existed in this system. Belov et al. [8] investigated the Al–Zn–Mg–Si systems by means of metallography, DSC, EPMA, X-ray spectroscopy and thermodynamical calculations, and found the presence of Al_3Ni and Mg_2Si particles could improve casting properties and mechanical properties. They also detected the boundaries among the phase fields of (Al), (Si), Mg_2Si and $Mg_3Zn_3Al_2$. Honda et al. [9] studied the solidification structure of the coating layer on hot-dip Zn–11%Al–3%Mg–0.2%Si-coated steel sheet by means of metallographic examinations together with calculation of phase diagram based on Thermo-Calc. Hausbrand et al. [10] discussed the corrosion of painted $MgZn_2$ with a defect, under constant conditions of high humidity and an electrolyte covered defect. It is well known that these useful phase equilibrium and thermodynamic information will help us design the optimal hot-dip aluminum–zinc coating alloy composition in order to control phase formation during the process of solidification and further improve the coating property.

This study focuses on the phase equilibria in the region where the major phases (Al), (Si), Mg_2Si and $MgZn_2$ coexist in the Al–Zn–Mg–Si system. The study strategy is to combine the calculation of phase diagrams (Calphad) with experiments. We first

* Corresponding author. Tel.: +86 21 56334045; fax: +86 21 56338065.
E-mail addresses: shuliqian@shu.edu.cn, qian246@hotmail.com (Q. Li).

0925-8388/$ – see front matter © 2010 Elsevier B.V. All rights reserved.
doi:10.1016/j.jallcom.2010.04.089

constructed the thermodynamic description of the Al–Zn–Mg–Si system from the constituent subsystems and calculated the phase equilibrium relations in the interesting region. The key alloy samples were selected based on the phase diagram calculated from the quaternary thermodynamic description. The samples were then studied by means of SEM, EDS, XRD and DSC to determine the phase relationships among the major phases of (Al), (Si), Mg_2Si and $MgZn_2$ in this system. The thermodynamic description of the Al–Zn–Mg–Si system was further improved by considering the experimental results in this work as well as those reported in the literature.

2. Binary and ternary systems

There are six binary subsystems in the Al–Zn–Mg–Si system: Al–Zn, Zn–Si, Al–Si, Al–Mg, Zn–Mg and Mg–Si, on which thermodynamic data were selected from literatures reported Al–Zn [11], Al–Si [11], Zn–Si [11], Al–Mg [12], Zn–Mg [12] and Mg–Si [13]. All these six constituent binary systems have been thermodynamically modeled in the literature. Both Al–Si and Zn–Si systems are simple eutectic systems. The Al–Zn system exhibits a miscibility gap in the Al-based face-centered cubic (*fcc*) phase below 624.5 K. There is no intermediate phase has been found in these three systems. Jacobs et al. [11] evaluated these three binary systems in their thermodynamic assessments of the Al–Zn–Si system. As both assessments lead to very close results, the one selected for the COST 507 database [14] as well as reported by the Jacobs et al. [11] was chosen in present work.

Following a detailed experimental investigation, Liang et al. [12] provided an assessment of the Al–Mg system. Their assessment has been included in the COST 507 database and will be used in the present study. The thermodynamic description of the Mg–Zn system has been first presented by Agarwal et al. [15]. The subsequent update on this binary by Liang et al. [12] is recommended since it agrees well with various types of experimental data such as phase diagram, enthalpy of mixing, heat capacity and chemical potential and also takes into account of the homogeneity range of the C14 Laves phase ($MgZn_2$). The description of the Mg–Zn binary system from Liang et al. [12] is adopted in this work.

The Mg–Si system has also been assessed several times [13,16]. While the Mg–Si phase diagram appears to be well established, the authors of these assessments emphasized the very large discrepancies in the thermodynamic data reported for this system. Two sets of descriptions assessed by Yan et al. [13] and Feufel et al. [16] are frequently adopted in different ternary systems. The Gibbs energy descriptions of the Mg_2Si phase in the two studies differ significantly. In this work, an appropriate description of Mg–Si system will be chosen based on our experimental results.

For the ternary Al–Zn–Si system, Jacobs et al. [11] calculated several isoplethal sections and compared with available experimental data. No ternary interaction parameters were used in their thermodynamic description.

The Al–Mg–Zn system has a relatively complex equilibrium relationship. Based on the large amount of the experiment information, thermodynamic descriptions of this ternary system have been provided by Liang et al. [12,17]. Because the more experimental information was considered, the description from Liang et al. [17] is more consistent with the experiment data and will be used in the present study.

No ternary compound has been found in the Al–Mg–Si system. Chakraborti et al. [18] proposed the first thermodynamic description for this system. New assessments were reported later by Feufel et al. [16] and Lacaze et al. [19] in which the description of Mg–Si system was assessed by Feufel et al. [16].

No ternary compound was found in the Zn–Mg–Si system either. The modified quasichemical model was used by Shukla et al. [20] to describe the liquid phase in the Zn–Mg–Si system, and the calculated result agreed with a partial section along the Mg_2Si–$MgZn_2$ join. Since the liquid phases in other constituent subsystems are all described by the Redlich-Kister type of solution model, the liquid phase in the Zn–Mg–Si system needs to be remodeled.

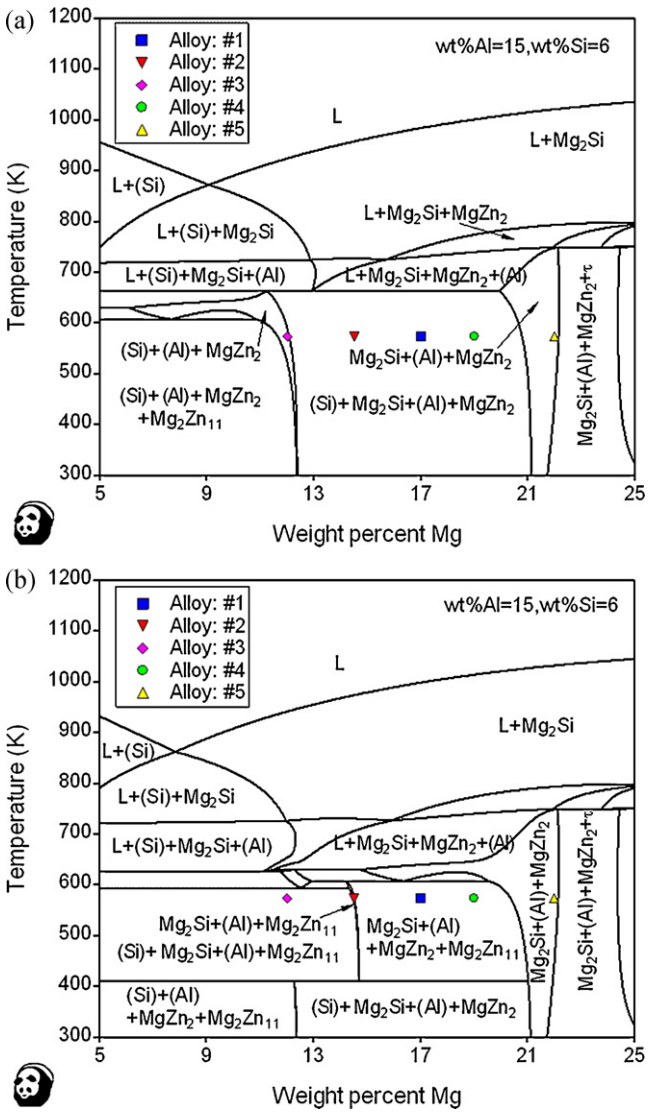

Fig. 1. Calculated isoplethal sections with 15 wt% Al and 6 wt% Si using different Mg–Si descriptions. (a) Mg–Si from Yan et al. [13]; (b) Mg–Si from Feufel et al. [16].

3. Selection of samples

The approach of thermodynamic modeling has been proved to be an efficient way to identify the key experiments that can provide the maximum amount of information on phase equilibria and drastically reduce the extensive experimental effort in a multicomponent system [21]. A strategy using thermodynamic modeling to aid the selection of key alloy compositions for experimental investigation was employed in this study. In the interested compositional range of Al–Zn based hot-dip alloys, the thermodynamic descriptions of Mg–Si from Yan et al. [13] and Feufel et al. [16] predicted different phase relationships in the Al–Zn–Mg–Si quaternary system. Experiments are designed to clarify this inconsistency. Two isoplethal sections of the Al–Zn–Mg–Si system with 15 wt% Al and 6 wt% Si were calculated with the Mg–Si description according to Yan et al. [13] and Feufel et al. [16], respectively. Fig. 1(a) and (b)

Table 1
The compositions of the selected alloys.

Sample	Compositions (wt%)				Weight (g)
	Al	Zn	Mg	Si	
#1	15	62	17	6	35
#2	15	64.5	14.5	6	35
#3	15	67	12	6	40
#4	15	60	19	6	35
#5	15	57	22	6	35

are two calculated diagrams. It can be seen that these two diagrams have significant difference in the phase relationships below 700 K. To verify the equilibrium relationships in this region, five alloy samples were prepared, which compositions are listed in Table 1 and also marked as symbols in Fig. 1(a) and (b).

4. Experimental investigation

All the starting materials used for the alloy samples were high purity: Al(99.99%), Zn(99.99%), Mg(99.99%) and Si(99.999%). Table 1 gives the compositions of the selected alloys which were labeled as #1, #2, #3, #4 and #5. The alloys were prepared in a medium frequency induction furnace under an argon atmosphere with ultrahigh purity (99.999% Ar). The Al–Si alloys were melted first and then Mg and Zn were added into the samples one by one to reduce the vaporization of Mg and Zn. If it was found that Mg or Zn content was smaller than the desired value, extra amount of Mg or Zn was added again into the sample. Each alloy was melted and flipped at least three times to promote complete mixing and melting. The final compositions of samples were confirmed by chemical analysis. Only the ingots with a weight loss of less than 1 wt% were chosen for further investigation. Samples were wire cut as the size of 10 mm × 10 mm × 5 mm. They were annealed in an ultrahigh purity argon atmosphere (99.999% Ar) at 573 K for 45 days and then water cooled to room temperature.

Powder X-ray diffraction (XRD) analysis was performed on the selected samples using a D/max 2500 diffractometer with CuK_{α} radiation to identify the crystal structures of phases. The microstructure of each sample was examined using a JSM-700IF scanning electron microscope (SEM) with back-scattered electrons (BSE) detector. The annealed samples were studied by DSC under an argon atmosphere at a heating rate of 5 K/min. The specimens for DSC, each of 10–20 mg, were put in alumina crucibles and heated in flowing argon at a flowing rate of 15 ml/min.

5. Results and discussion

5.1. Multiphase equilibria at 573 K

The crystal structure of each phase was identified by the X-ray diffraction technique. The XRD diffraction patterns of the five samples were shown in Fig. 2, from which it can be seen that the four-phase equilibrium of (Al) + (Si) + Mg_2Si + $MgZn_2$ was observed in the samples #1, #2 and #4. The samples #3 and #5 displayed two three-phase equilibria of (Al) + (Si) + $MgZn_2$ and (Al) + Mg_2Si + $MgZn_2$, respectively.

The BSE images of the samples were shown in Fig. 3. According to the EDS measurement on the phase compositions of the sample #1, as shown in Fig. 3, the brightest phases are $MgZn_2$, gray phases are (Al) solid solution, the smallest gray dark phases are (Si) solid solution and the black phases are Mg_2Si. The phases in the samples #2, #3, #4 and #5 have also been identified by EDS. The results show non-existence of quaternary compound in these alloy samples.

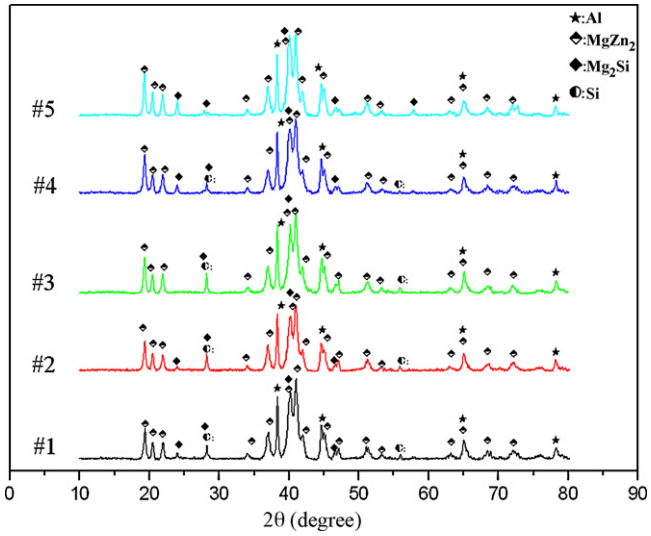

Fig. 2. X-ray diffraction patterns of the cast alloys #1–#5 after annealing at 573 K for 45 days.

Table 3
Comparison between the phase transition temperatures characterized by DSC and those predicted from calculation.

Sample	DSC (K)	Predicted from calculation (K)	
		See Fig. 1(a)	See Fig. 1(b)
#1	655	663	593
#3	655		607

Based upon the information from the BSE images, XRD and EDS, the phases observed in the alloy samples are summarized in Table 2. For comparison, Table 2 also lists the phases in equilibrium predicted from the model calculated as shown in Fig. 1(a) and (b). It can be seen from this table that the current experimental results support the calculated phase relationships in Fig. 1(a).

5.2. Phase transition temperature

Further experiments were carried out to study the phase transition temperature between 350 K and 700 K by DSC. Fig. 4 is the DSC heating curves of the alloys #1 and #3. Two curves both present endothermic peaks, which indicate that there is a phase transition. The transition temperature is 655 K for alloy #1 and alloy #3, which indicates that they could represent the same phase transition temperature. Careful examination of Fig. 1(a) tells us that there is an invariant phase transition at 663 K involving liquid phase. Both the compositions of the alloys #1 and #3 are within the invariant reaction. Corresponding to these two compositions, Fig. 1(b) predicts two different phase transition temperatures where liquid phase starts to form and Table 3 lists these temperatures. This also confirms that the calculation in Fig. 1(a) agrees with current experimental results and the thermodynamic description of the Mg–Si

Table 2
Comparison between the phases observed from the annealed alloys and those predicted from phase diagram calculations.

Sample	Phases characterized by XRD and SEM-EDS	Phases predicted from calculated diagrams	
		See Fig. 1(a)	See Fig. 1(b)
#1	(Al) + (Si) + $MgZn_2$ + Mg_2Si	(Al) + (Si) + $MgZn_2$ + Mg_2Si	(Al) + Mg_2Zn_{11} + $MgZn_2$ + Mg_2Si
#2	(Al) + (Si) + $MgZn_2$ + Mg_2Si	(Al) + (Si) + $MgZn_2$ + Mg_2Si	(Al) + Mg_2Si + Mg_2Zn_{11}
#3	(Al) + (Si) + $MgZn_2$	(Al) + (Si) + $MgZn_2$	(Al) + (Si) + Mg_2Zn_{11} + Mg_2Si
#4	(Al) + (Si) + $MgZn_2$ + Mg_2Si	(Al) + (Si) + $MgZn_2$ + Mg_2Si	(Al) + Mg_2Zn_{11} + $MgZn_2$ + Mg_2Si
#5	(Al)+ $MgZn_2$ + Mg_2Si	(Al)+ $MgZn_2$ + Mg_2Si	(Al) +$MgZn_2$ + Mg_2Si

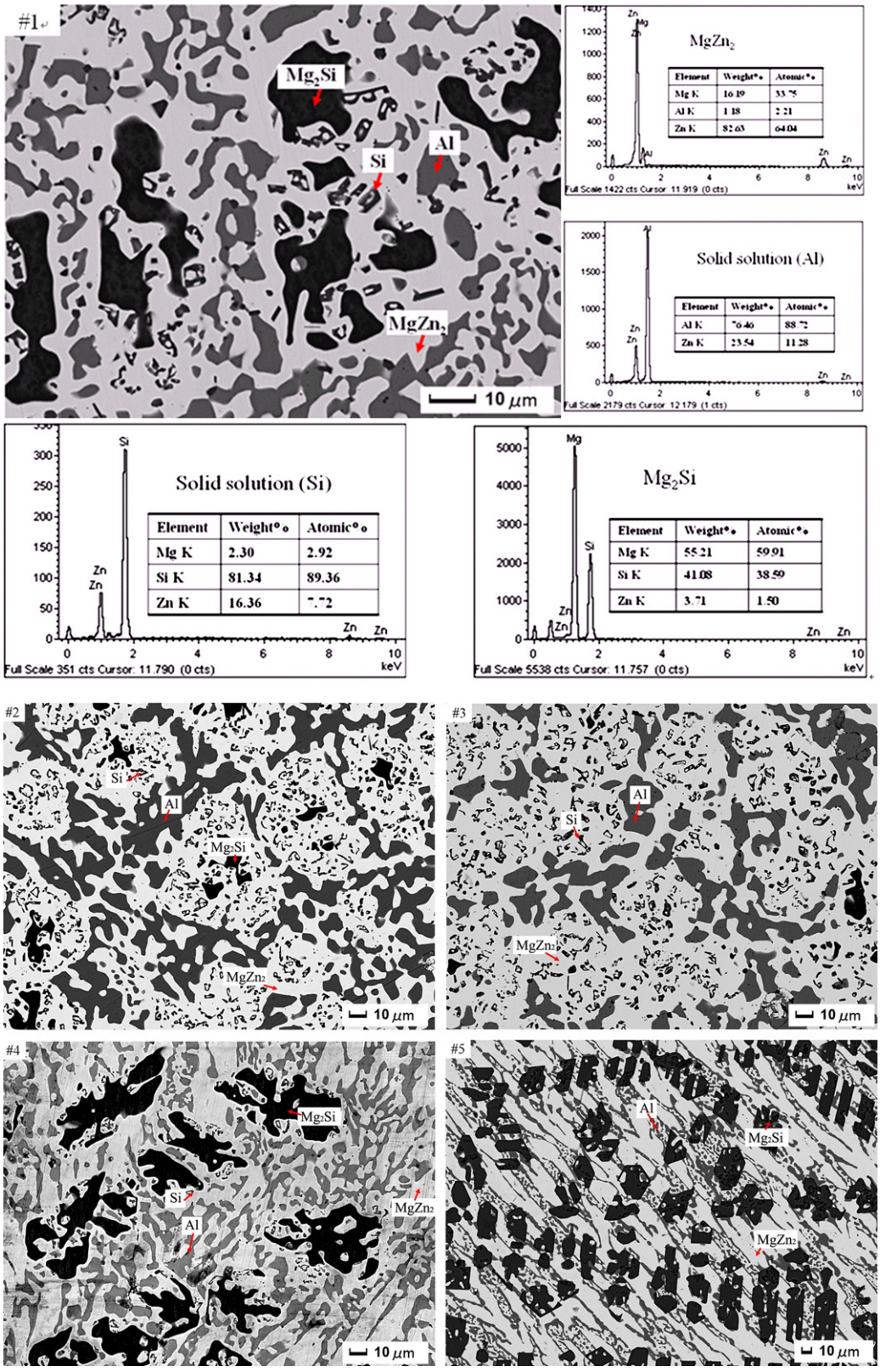

Fig. 3. BSE image of alloy #1 annealed at 573 K with EDS results and BSE images of alloy #2–#5 annealed at 573 K.

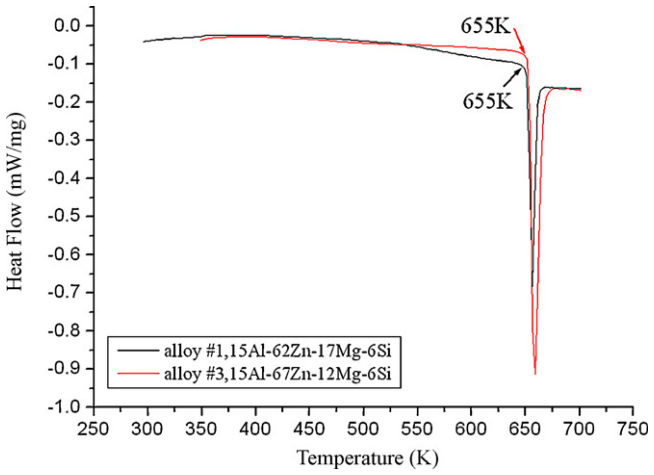

Fig. 4. The DSC heating curves of alloys annealed for 45 days.

system provided by Yan et al. [13] is appropriate for describing the Al–Zn–Mg–Si system.

6. Thermodynamic modeling

6.1. Assessment on liquidus parameters of ternary systems

The thermodynamic description of the Mg–Si system assessed by Yan et al. [13] will be used in this study and the ternary interaction parameters for the liquid phase in the Al–Mg–Si and Zn–Mg–Si systems will be reassessed using the current experimental results.

The liquid phase is described by a substitutional solution model for which the Gibbs energy is given as follows:

$$G^{Liq} = x_{Al}G^{\circ,liq}_{Al} + x_{Zn}G^{\circ,liq}_{Zn} + x_{Mg}G^{\circ,Liq}_{Mg} + x_{Si}G^{\circ,Liq}_{Si} + RT(x_{Al}\ln x_{Al} + x_{Zn}\ln x_{Zn} + x_{Mg}\ln x_{Mg} + x_{Si}\ln x_{Si}) + G^{ex,Liq} \quad (1)$$

where x_i and $G^{\circ,liq}_i$ represent the mole fraction and the molar Gibbs energy of the pure component i in the liquid phase, respectively, R is gas constant, T is the absolute temperature and $G^{ex,Liq}$ is the excess Gibbs energy. The ternary excess Gibbs energy of the liquid phase in the Al–Mg–Si system is presented by

$$G^{ex,Liq}_{Al,Mg,Si} = x_{Al}x_{Mg}x_{Si}(L^0_{(Al,Mg,Si)}x_{Al} + L^1_{(Al,Mg,Si)}x_{Mg} + L^2_{(Al,Mg,Si)}x_{Si}) \quad (2)$$

Considering the experimental data from the work by Schürmann et al. [22], Feufel et al. [16] and Hanson et al. [23], the ternary interaction parameters were assessed to be $L^0_{(Al,Mg,Si)} = 45000$, $L^1_{(Al,Mg,Si)} = -34000 + 15T$, $L^2_{(Al,Mg,Si)} = -35000 - 3T$. Figs. 5–7 compare the calculated phase diagrams with those experimental data, which indicate that good agreement has been reached between calculation and the experimental data.

For the Mg–Zn–Si system, its ternary excess Gibbs energy of the liquid phase is presented as:

$$G^{ex,Liq}_{Mg,Zn,Si} = x^2_{Mg}x_{Zn}x_{Si}L^0_{(Mg,Zn,Si)} \quad (3)$$

Considering the experimental data of a partial section along the Mg_2Si–$MgZn_2$ join studied by Bollenrath et al. [24], the ternary interaction parameter is assessed to be $L^0_{(Mg,Zn,Si)} = -44083 + 22.5T$. Fig. 8 shows that the calculated diagram agrees well with the experimental data. All parameters in the thermodynamic descriptions of the Al–Zn–Mg–Si quaternary system are listed in Table 4.

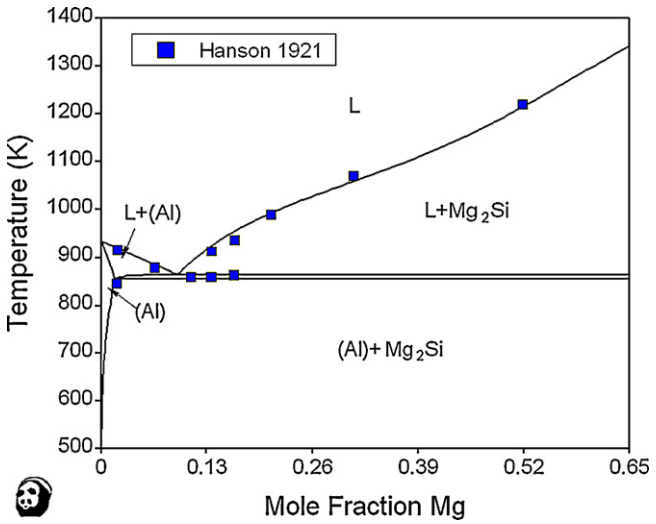

Fig. 5. Calculated isopleth of Al–Mg–Si system from Al to Mg_2Si with experimental data [23].

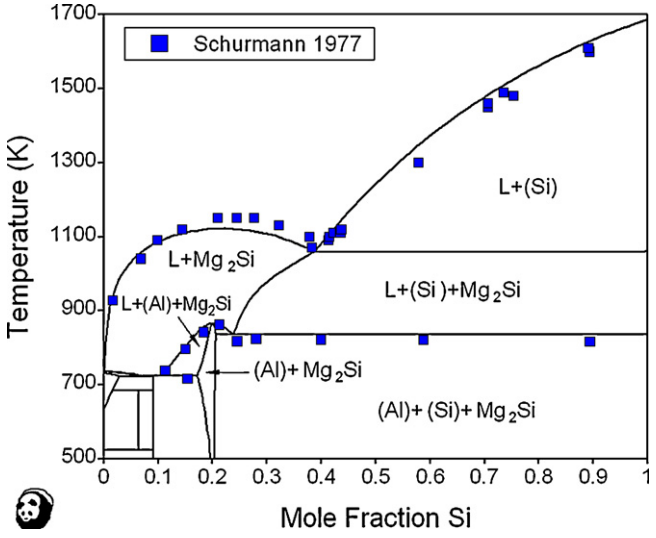

Fig. 6. Calculated isopleth of Al–Mg–Si system from $Mg_{51}Al_{49}$ to Si with experimental data [22].

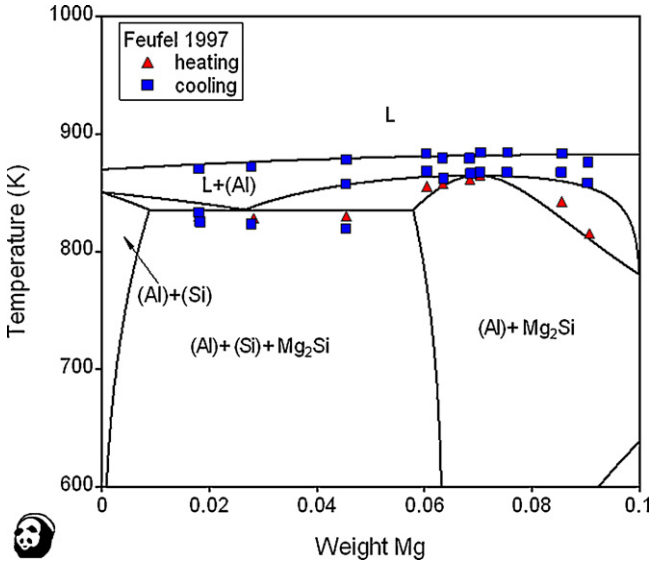

Fig. 7. Calculated isopleth of Al–Mg–Si system at 95 wt% Al with experimental data [16].

Table 4
The thermodynamic parameters of the Al–Zn–Mg–Si quaternary system reported in the literature and optimized in this study. Parameters are given as $a+bT+cT\ln(T)+dT^2+e/T+fT^3$ in J mol^{-1} (in J/mol of the formula unit).

Parameter	*a*	*b*	*c*	*d*	Ref.
Liquid, Redlich-kister-Muggianu					
$^0L_{Al,Si}$	−11655.93	−0.92934			[11]
$^1L_{Al,Si}$	−2873.45	0.29450			[11]
$^2L_{Al,Si}$	2520				[11]
$^0L_{Al,Mg}$	−12000	8.566			[12]
$^1L_{Al,Mg}$	1894	−3			[12]
$^2L_{Al,Mg}$	2000				[12]
$^0L_{Al,Zn}$	10465.55	−3.39259			[11]
$^0L_{Mg,Si}$	−73623.6	27.3211			[13]
$^1L_{Mg,Si}$	−30000	21.4382			[13]
$^2L_{Mg,Si}$	44417.4	−28.3755			[13]
$^0L_{Mg,Zn}$	−77729.2	680.523	95	0.04	[12]
$^1L_{Mg,Zn}$	3674.72	0.57139			[12]
$^2L_{Mg,Zn}$	−1588.15				[12]
$^0L_{Si,Zn}$	7829.25				[11]
$^1L_{Si,Zn}$	−3338.18				[11]
$^2L_{Si,Zn}$	−891.33				[11]
$^0L_{Al,Mg,Si}$	45000				This work
$^1L_{Al,Mg,Si}$	−34000	15			This work
$^2L_{Al,Mg,Si}$	−35000	−3			This work
$^0L_{Al,Mg,Zn}$	−11475	11			[17]
$^1L_{Al,Mg,Zn}$	−11475	11			[17]
$^2L_{Al,Mg,Zn}$	−11475	11			[17]
$^0L_{Mg,Si,Zn}$	−44083	22.5			This work
(Al), Redlich-kister-Muggianu					
$^0L_{Al,Si}$	−3423.91	−0.09584			[11]
$^0L_{Al,Mg}$	4971	−3.5			[12]
$^1L_{Al,Mg}$	900	0.423			[12]
$^2L_{Al,Mg}$	950				[12]
$^0L_{Al,Zn}$	7297.48	0.47512			[11]
$^1L_{Al,Zn}$	6612.88	−4.5911			[11]
$^2L_{Al,Zn}$	−3097.19	3.30635			[11]
$^0L_{Mg,Si}$	−7148.79	0.89361			[13]
$^0L_{Mg,Zn}$	−3056.82	5.63801			[12]
$^1L_{Mg,Zn}$	−3127.26	5.65563			[12]
$^0L_{Si,Zn}$	50000				[11]
(Mg), Redlich-kister-Muggianu					
$^0G_{Al}{}^{HCP\text{-}A3}$_$^0G_{Al}{}^{FCC}$	5481	−1.8			[25]
$^0G_{Zn}{}^{HCP\text{-}A3}$_$^0G_{Zn}{}^{HCP}$	2969.82	−1.56968			[26]
$^0L_{Al,Si}$	50000				[11]
$^0L_{Al,Mg}$	1950	−2			[12]
$^1L_{Al,Mg}$	1480	−2.08			[12]
$^2L_{Al,Mg}$	3500				[12]
$^0L_{Al,Zn}$	18820.95	−8.95255			[11]
$^1L_{Al,Zn}$	−702.79				[11]
$^0L_{Mg,Zn}$	−3056.82	5.63801			[12]
$^1L_{Mg,Zn}$	−3127.26	5.65563			[12]
$^0L_{Mg,Si}$	−7148.79	0.894			[13]
$^0L_{Si,Zn}$	50000				[11]
(Zn), Redlich-kister-Muggianu					
$^0G_{Al}{}^{HCP\text{-}Zn}$ _$^0G_{Al}{}^{FCC}$	5481	−1.8			[25]
$^0G_{Mg}{}^{HCP\text{-}A3}$_$^0G_{Mg}{}^{HCP}$	100				[17]
$^0L_{Al,Si}$	50000				[11]
$^0L_{Al,Mg}$	1950	−2			[12]
$^1L_{Al,Mg}$	1480	−2.08			[12]
$^2L_{Al,Mg}$	3500				[12]
$^0L_{Al,Zn}$	18820.95	−8.95255			[11]
$^1L_{Al,Zn}$	−702.79				[11]
$^0L_{Mg,Zn}$	−3056.82	5.63801			[12]
$^1L_{Mg,Zn}$	−3127.26	5.65563			[12]
$^0L_{Mg,Si}$	−7148.79	0.894			[13]
$^0L_{Si,Zn}$	50000				[11]
(Si), Redlich-kister-Muggianu					
$^0G_{Al}{}^{DIAMOND\text{-}A4}$ _$^0G_{Al}{}^{FCC}$		30			[11]
$^0G_{Zn}{}^{DIAMOND\text{-}A4}$ _$^0G_{Al}{}^{HCP}$		30			[11]
$^0L_{Al,Si}$	111417.70	−46.13920			[11]
$^0L_{Si,Zn}$	100000				[11]
$^0L_{Al,Zn}$	100000				[11]

Table 4 (*Continued*)

Parameter	*a*	*b*	*c*	*d*	Ref.
$MgZn_2$, compound energy formalism, (Al, Mg, Zn)(Al, Mg, Zn)$_2$					
${}^0G_{*:*}^{MgZn2} - 3{}^0G_{*}^{SER}$	15000.00				[17]
${}^0G_{Mg:Al}^{MgZn2} - {}^0G_{Mg}^{HCP} - 2{}^0G_{Al}^{FCC}$	12671.10	16.8			[27]
${}^0G_{Zn:Al}^{MgZn2} - {}^0G_{Zn}^{HCP} - 2{}^0G_{Al}^{FCC}$	15000.00				[17]
${}^0G_{Al:Mg}^{MgZn2} - {}^0G_{Al}^{FCC} - 2{}^0G_{Mg}^{HCP}$	37328.9	−16.8			[27]
${}^0G_{Zn:Mg}^{MgZn2} - {}^0G_{Zn}^{HCP} - 2{}^0G_{Mg}^{HCP}$	65355.45	−8.83886			[17]
${}^0G_{Al:Zn}^{MgZn2} - {}^0G_{Al}^{FCC} - 2{}^0G_{Zn}^{HCP}$	15000.00				[17]
${}^0G_{Mg:Zn}^{MgZn2} - {}^0G_{Mg}^{HCP} - 2{}^0G_{Zn}^{HCP}$	−35355.45	8.83886			[17]
${}^0L_{Mg,Zn:*}^{MgZn2}$	8000.00				[17]
${}^0L_{*:Mg,Zn}^{MgZn2}$	35000.00				[17]
${}^0L_{Mg,Al:*}^{MgZn2}$	15000.00				[27]
${}^0L_{*:Mg,Al}^{MgZn2}$	8000.00				[27]
${}^0L_{*:Al,Zn}^{MgZn2}$	−7500.00	−18.00			[17]
τ-phase, compound energy formalism, $Mg_{26}(Mg, Al)_6(Al, Mg, Zn)_{48}Al$					
${}^0G_{Mg:Mg:Al:Al}^{\tau} - 49{}^0G_{Al}^{FCC} - 32{}^0G_{Mg}^{HCP}$	−81000.00	−186.30			[17]
${}^0G_{Mg:Mg:Zn:Al}^{\tau} - {}^0G_{Al}^{FCC} - 32{}^0G_{Mg}^{HCP} - 48{}^0G_{Zn}^{HCP}$	−811620.0	162.00			[17]
${}^0G_{Mg:Mg:Mg:Al}^{\tau} - {}^0G_{Al}^{FCC} - 80{}^0G_{Mg}^{HCP}$	405000.00	243.00			[17]
${}^0G_{Mg:Al:Al:Al}^{\tau} - 55{}^0G_{Al}^{FCC} - 26{}^0G_{Mg}^{HCP}$		−105.30			[17]
${}^0G_{Mg:Al:Zn:Al}^{\tau} - 7{}^0G_{Al}^{FCC} - 26{}^0G_{Mg}^{HCP} - 48{}^0G_{Zn}^{HCP}$	−832680.0	162.00			[17]
${}^0G_{Mg:Al:Mg:Al}^{\tau} - 7{}^0G_{Al}^{FCC} - 74{}^0G_{Mg}^{HCP}$	1053000.0	405.00			[17]
${}^0L_{Mg:Mg:Al,Zn:Al}^{\tau}$	−105300.0	243.00			[17]
${}^0L_{Mg:Mg:Al,Mg:Al}^{\tau} = {}^0L_{Mg:Al:Al,Mg:Al}^{\tau}$	−202500.0	−40.50			[17]
${}^0L_{Mg:Mg:Mg,Zn:Al}^{\tau} = {}^0L_{Mg:Al:Mg,Zn:Al}^{\tau}$	243000.0	81.00			[17]
${}^0L_{Mg:Al:Al,Zn:Al}^{\tau}$	−16200.0	243.00			[17]
Φ-phase, compound energy formalism, $Mg_6(Al, Zn)_5$					
${}^0G_{Mg:Al}^{\Phi} - 6{}^0G_{Mg}^{HCP} - 5{}^0G_{Al}^{FCC}$	−15400.0	−16.50			[17]
${}^0G_{Mg:Zn}^{\Phi} - 6{}^0G_{Mg}^{HCP} - 5{}^0G_{Zn}^{HCP}$	−79530.0	20.90			[17]
${}^0L_{Mg:Al,Zn}^{\Phi}$	−23100.0	11.00			[17]
$Al_{30}Mg_{23}$, compound energy formalism, $Mg_{23}(Al, Zn)_{30}$					
${}^0G_{Mg:Al}^{Al30Mg23} - 23{}^0G_{Mg}^{HCP} - 30{}^0G_{Al}^{FCC}$	−52565.4	−173.1775			[17]
${}^0G_{Mg:Zn}^{Al30Mg23} - 23{}^0G_{Mg}^{HCP} - 30{}^0G_{Zn}^{FCC}$	−318000.0	−63.600			[17]
Al_3Mg_2, compound energy formalism, $Mg_{89}(Al, Zn)_{140}$					
${}^0G_{Mg:Al}^{Al3Mg2} - 89{}^0G_{Mg}^{HCP} - 140{}^0G_{Al}^{FCC}$	−246175.0	−675.55			[17]
${}^0G_{Mg:Zn}^{Al3Mg2} - 89{}^0G_{Mg}^{HCP} - 140{}^0G_{Zn}^{HCP}$	206100.0				[17]
${}^0L_{Mg:Al,Zn}^{Al3Mg2}$	−1717500	343.50			[17]
$Al_{12}Mg_{17}$, compound energy formalism, $Mg_{10}(Mg, Al, Zn)_{24}(Al, Mg, Zn)_{24}$					
${}^0G_{Mg:Al:Al}^{Al12Mg17} - 10{}^0G_{Mg}^{HCP} - 48{}^0G_{Al}^{FCC}$	195750.0	−203.00			[17]
${}^0G_{Mg:Mg:Al}^{Al12Mg17} - 34{}^0G_{Mg}^{HCP} - 24{}^0G_{Al}^{FCC}$	−105560.0	−101.5			[17]
${}^0G_{Mg:Al:Mg}^{Al12Mg17} - 34{}^0G_{Mg}^{HCP} - 24{}^0G_{Al}^{FCC}$	568249.2	−276.138			[17]
${}^0G_{Mg:Mg:Mg}^{Al12Mg17} - 58{}^0G_{Mg}^{HCP}$	266939.2	−174.6380			[17]
${}^0G_{Mg:Zn:Al}^{Al12Mg17} - 10{}^0G_{Mg}^{HCP} - 24{}^0G_{Al}^{FCC} - 24{}^0G_{Zn}^{HCP}$	−174000.0	116.00			[17]
${}^0G_{Mg:Mg:Zn}^{Al12Mg17} - 34{}^0G_{Mg}^{HCP} - 24{}^0G_{Zn}^{HCP}$	−290000.0	116.00			[17]
${}^0G_{Mg:Zn:Mg}^{Al12Mg17} - 34{}^0G_{Mg}^{HCP} - 24{}^0G_{Zn}^{HCP}$	198599.2	42.8620			[17]
${}^0G_{Mg:Al:Zn}^{Al12Mg17} - 10{}^0G_{Mg}^{HCP} - 24{}^0G_{Al}^{FCC} - 24{}^0G_{Zn}^{HCP}$	11310.0	14.50			[17]
${}^0G_{Mg:Zn:Zn}^{Al12Mg17} - 10{}^0G_{Mg}^{HCP} - 48{}^0G_{Zn}^{HCP}$	580000.0				[17]
${}^0L_{Mg:Al:Al,Mg}^{Al12Mg17} = {}^0L_{Mg:Mg:Al,Mg}^{Al12Mg17} = {}^0L_{Mg:Zn:Al,Mg}^{Al12Mg17}$	226200.0	−29.00			[17]
${}^0L_{Mg:Mg,Zn:Al}^{Al12Mg17} = {}^0L_{Mg:Mg,Zn:Mg}^{Al12Mg17} = {}^0L_{Mg:\ Mg,Zn:Zn}^{Al12Mg17}$	−232000.0	116.00			[17]
Mg_2Zn_{11}, compound energy formalism, $Mg_2(Zn, Al)_{11}$					
${}^0G_{Mg:Zn}^{Mg2Zn11} - 2{}^0G_{Mg}^{HCP} - 11{}^0G_{Zn}^{HCP}$	−73818.32	18.45457			[17]
${}^0G_{Mg:Zn}^{Mg2Zn11} - 2{}^0G_{Mg}^{HCP} - 11{}^0G_{Al}^{FCC}$	130000.0	−26.00			[17]
Mg_2Zn_3, compound energy formalism, $Mg_2(Zn, Al)_3$					
${}^0G_{Mg:Zn}^{Mg2Zn3} - 2{}^0G_{Mg}^{HCP} - 3{}^0G_{Zn}^{HCP}$	−54406.20	13.60156			[17]
${}^0G_{Mg:Al}^{Mg2Zn3} - 2{}^0G_{Mg}^{HCP} - 3{}^0G_{Al}^{FCC}$	1000.00	−0.20			[17]
MgZn, compound energy formalism, $Mg_{12}(Zn, Al)_{13}$					
${}^0G_{Mg:Zn}^{MgZn} - 12{}^0G_{Mg}^{HCP} - 13{}^0G_{Zn}^{HCP}$	−236980.84	59.24524			[17]
${}^0G_{Mg:Zn}^{MgZn} - 12{}^0G_{Mg}^{HCP} - 13{}^0G_{Al}^{FCC}$	−10000.0	2.50			[17]
Mg_7Zn_3, stoichiometric, $Mg_{51}Zn_{20}$					
${}^0G_{Mg:Zn}^{Mg7Zn3} - 51{}^0G_{Mg}^{HCP} - 20{}^0G_{Zn}^{HCP}$	−335741.54	35.50			[17]
Mg_2Si, stoichiometric, Mg_2Si					
${}^0G_{Mg:Si}^{Mg2Si} - 2{}^0G_{Mg}^{HCP} - {}^0G_{Si}^{DIAMOND-A4}$	−64110	14.868			[13]

6.2. Thermodynamic calculation of the Al–Zn–Mg–Si system

Based on the thermodynamic descriptions of the Al–Zn–Mg [17] and Al–Zn–Si [11] from literature, and those of the Al–Mg–Si and Zn–Mg–Si systems assessed in this work, the thermodynamic description of the quaternary Al–Zn–Mg–Si system was extrapolated from these four ternary systems. To validate this quaternary description, several calculations were made below and compared with the available experimental data.

Sebkova et al. [28] measured the activities of Mg in several liquid alloys in the Al–Zn–Mg–Si system at 1073 K. These alloys have different compositions for the same component. Fig. 9 shows the activities of Mg versus mole fraction of only Al, where the solid squares are the experimental results [28] and the open squares are

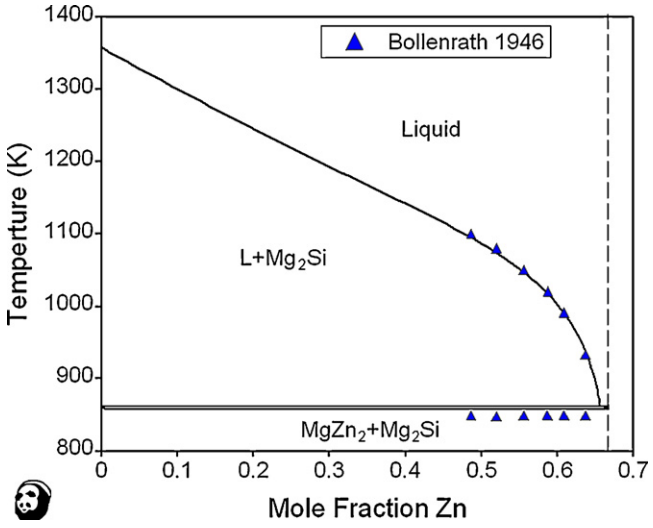

Fig. 8. Calculated isopleth of Zn–Mg–Si system from Mg_2Si to $MgZn_2$ with experimental data [24].

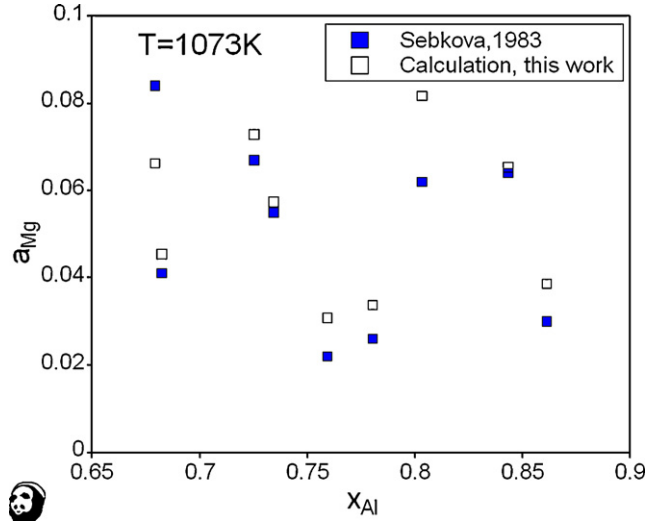

Fig. 9. Comparison of activities of Mg in liquid phase of the Al–Zn–Mg–Si system at 1073 K.

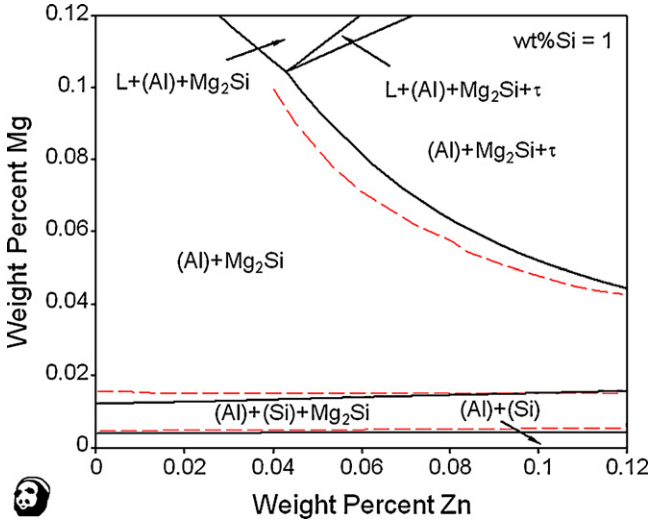

Fig. 10. Isothermal section in the Al corner of the Al–Zn–Mg–Si system at 733 K with 1 wt% Si.

the calculated values. Comparison shows that a reasonable agreement has been obtained.

Using the metallographic method Axon et al. [29] studied the phase relationships near the Al-rich corner in an isothermal section of Al–Zn–Mg–Si with 1 wt% Si at 733 K and proposed the phase boundaries in this corner. Fig. 10 is the calculated isothermal section with the experimental phase boundaries proposed by Axon et al. [29] and their agreement is within 0.01 wt%.

7. Conclusions

A thermodynamic description of the quaternary system Al–Zn–Mg–Si was developed in this study and validated by experimental measurements. The multiphase equilibria among (Al), (Si), Mg_2Si and $MgZn_2$ at 573 K were well established through both experimental measurements and thermodynamic calculations. Two three-phase equilibria, (Al) + (Si) + $MgZn_2$ and (Al) + Mg_2Si + $MgZn_2$, are separated by the four-phase equilibrium (Al) + (Si) + Mg_2Si + $MgZn_2$. The experimental results suggest the appropriate selection of the thermodynamic description of the Mg–Si system. The interaction parameters in the liquid phase of ternary Al–Mg–Si and Zn–Mg–Si systems have been assessed based on the experimental data. The thermodynamic description of the quaternary Al–Zn–Mg–Si system was extrapolated from the related constituent ternary systems. Calculations were made to compare with the available experimental data and a good agreement has been reached. The thermodynamic description of the Al–Zn–Mg–Si system can be used as a reliable tool to guide the alloy design for the alloys with the major phases (Al), (Si), Mg_2Si and $MgZn_2$ such as the ZA27 and Al–Zn based hot-dip alloys.

Acknowledgments

The authors would like to thank the financial supports from Chinese National Key Technology R & D Program (2007BAE09B03), Key Science and Technology Development Program in the Eleventh Five-Year Plan of Guizhou Province (20076003), Science and Technology Commission of Shanghai Municipality (09195802700) and Aluminum Corporation of China (Science and Technology Development Fund, 2007KJA07).

References

[1] W.J. Lai, Y.Y. Li, Y.F. Hsu, S. Trong, W.H. Wang., J. Alloys Compd. 476 (2009) 118–124.
[2] S.W. Pan, F.C. Yin, M.X. Zhao, Y. Liu, X.P. Su., J. Alloys Compd. 470 (2009) 600–605.
[3] D. Kevorkov, M. Pekguleryuz, J. Alloys Compd. 478 (2009) 427–436.
[4] C.H. Niederberger, J. Michler, A. Jacot, Acta Mater. 56 (2008) 4002–4011.
[5] J. Tanaka, K. Ono, S. Hayashi, K. Ohsasa, T. Narita, ISIJ Int. 42 (2002) 80–85.
[6] Y. Morimoto, K. Honda, K. Nishimura, S. Tanaka, A. Takahashi, H. Shindo, M. Kurosaki, Nippon Steel Technical Report, 87 (2003) 24–27.
[7] G.Y. Yuan, Z.L. Liu, Q.D. Wang, W.J. Ding., Mater. Lett. 56 (2002) 53–58.
[8] N.A. Belov, V.V. Cheverikin, D.G. Eskin, A.N. Turchin., Mater. Sci. Forum 519–521 (2006) 413–418.
[9] K. Honda, W. Yamada, K. Ushioda, Mater. Trans. 49 (2008) 1395–1400.
[10] R. Hausbrand, M. Stratmann, M. Rohwerder, Corros. Sci. 51 (2009) 2107–2114.
[11] M.H.G. Jacobs, P.J. Spencer, Calphad 20 (1996) 307–320.
[12] H. Liang, S.L. Chen, Y.A. Chang, Metall. Mater. Trans. A 28 (1997) 1725–1734.
[13] X.Y. Yan, F. Zhang, Y.A. Chang, J. Phase Equilib. 21 (2000) 379–384.
[14] I. Ansara, European Commission, Brussels and Luxembourg, 1998, pp. 18171–18175.
[15] R. Agarwal, T.G. Chart, G. Effenberg, S.G. Fries, H.L. Lukas, G. Petzow, E. Sommer, Z. Metallkd. 83 (1992) 216–223.
[16] H. Feufel, T. Gödecke, H.L. Lukas, F. Sommer, J. Alloys Compd. 247 (1997) 31–42.
[17] P. Liang, T. Tarfa, J.A. Robinson, S. Wagner, P. Ochin, M.G. Harmelin, H.J. Seifert, H.L. Lukas, F. Aldinger, Thermochim. Acta 314 (1998) 87–110.

[18] N. Chakraborti, H.L. Lukas, Calphad 16 (1992) 79–86.
[19] J. Lacaze, R.M. Valdes, Monatshefte für Chemie 136 (2005) 1899–1904.
[20] A. Shukla, Y.B. Kang, A.D. Pelton, Calphad 32 (2008) 470–477.
[21] Y. Yang, Y.A. Chang, L. Tan, W. Cao., Acta Mater. 53 (2005) 1711–1720.
[22] E. Schürmann, A. Fischer, Giessereiforschung 29 (1977) 161–165.
[23] D. Hanson, M.L.V. Gayler, J. Inst. Met. 26 (1921) 321–329.
[24] F. Bollenrath, H. Gröber, Z. Metallkd. 37 (1946) 116–126.
[25] A.T. Dinsdale, Calphad 15 (1991) 317–425.
[26] M. Kowalski, P.J. Spencer, J. Phase Equilib. 14 (1993) 432–438.
[27] T. Buhler, S.G. Fries, P.J. Spencer, H.L. Lukas, J. Chim. Phys. 94 (1997) 1043–1048.
[28] J. Sebkova, M. Beranek, Koveve Mater. 21 (1983) 228–240.
[29] H.J. Axon, W. Hume-Rothery, J. Inst. Met. 74 (1948) 315–329.